# A Narrow Vertical Beam Based Structure for Passive Pressure Measurement Using Two-Material 3D Printing

Hongliang Shi

***Abstract*—This paper presents a novel narrow vertical beam based structure for pressure measurement. The structure is designed to measure a target impact pressure which is associated with the maximum allowed force applied on the vertical beams. By varying the geometric parameters of the vertical beam, the structure is designed to measure the different target pressure. This structure is featured for a small size, disposable and low-cost design by means of 3D printing. Compared with the structure of a horizontal cantilever beam, the vertical beam structure has higher stiffness, clearer sign of failure. The maximum allowed force is derived from the analysis of buckling and maximum strength. With the analytical model, the sensor is set to measure the impact pressure of 1 $N/mm^2$. A stiffness matrix of the sensor is derived by means of the Screw Theory. One application example of the pressure sensor is proposed.**

***Index Terms*—beam structure, buckling, pressure sensor, 3D printing**

## I. Introduction

Pressure sensor is widely used in industry for structural loading, gas and liquid pressure measurement. According to the measurement algorithms, the pressure sensor can be categorized as passive and active sensors. Most pressure sensors are used to measure the variation of the pressure. On the contrary, some are designed to measure a target pressure or to be used as a switch.

Much work has been done in the design of pressure sensor. Sander et al.[1] designed a monolithic capacitive sensor. Someya et al.[2] designed a flexible pressure sensor matrix for the application of artificial skin. A lot of Micro-electro-mechanical Systems (MEMS) designs are proposed for the sensing [3], [4], [5], [6], [7], [8]. However, the cost of these pressure sensors are high. Additive manufacturing is widely used for rapid fabrication. Based on additive manufacturing, we can build the sensors in a low cost. The most common 3D fabrication of polymer objects is Fused Deposition Modeling (FDM). Some other 3D fabrication methods like selective laser melting (SLM), selective Laser Sintering (SLS), fused filament fabrication (FFF) and stereolithography (SLA) can be used for some other materials or for a higher precision. However, the cost is higher than FDM.

As shown in Fig. 1, we propose a structural sensor design with the application of the narrow vertical beams, which is built by 3D printing with main and supporting material. The pressure sensor can be mounted underneath a target object to passively measure whether the loading reaches a predesigned target pressure. The adoption of vertical beams increases the maximum allowed pressure compared to the application of horizontal beams. This also improves the stiffness of the structural sensor. However, it is more difficult to fabricate the vertical beam compared with the horizontal beam in the 3D fabrication. The rest of the paper is organized as follows: Section II illustrates the design algorithm. Section III presents the fabrication method using two kinds of plastic material. One is main material and the other is supporting material. In section IV, we derive the analytical model to calculate the maximum allowed force which is associated with the derivation of the target pressure for a single pressure cell. The stiffness matrices are derived for the analysis of the structure. In section V, one application of the structure is proposed. It is mounted underneath a biosimulant artifact to measure the pressure for a robot impact testing. A conclusion is made in Section VI.

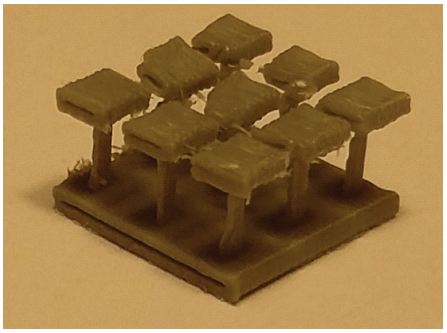

(a) Pressure Sensor of Vertical Beams

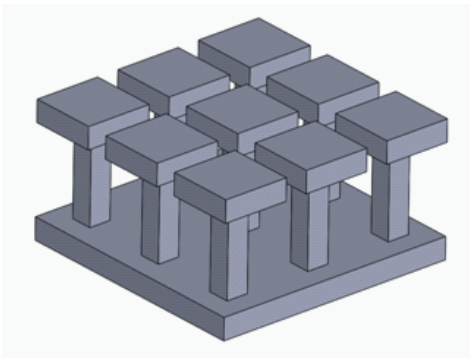

(b) Schematic Drawing of the Design

Fig. 1. Design of Pressure Sensor Structure.

## II. DESIGN

As shown in Fig. 2, the structural sensor system consists of two parts: the center structural sensor and a rigid disc. The grey structural sensor will be deformed or destroyed at the

Manuscript received Aug 12, 2015; revised Aug 20, 2015.

Hongliang Shi is with the Mechanical Engineering and Aerospace Department, The Ohio State University, Columbus, OH 43210, USA. Corresponding author. (e-mail: shi.347@osu.edu).

ISBN: 978-988-19253-6-7
ISSN: 2078-0958 (Print); ISSN: 2078-0966 (Online)

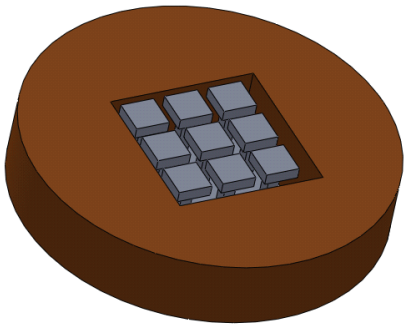

Fig. 2. Rigid Plate with Center Sensor Structure.

target pressure while the brown rigid plate has no significant deformation during testing. After each pressure testing, the grey structural sensor is disposed and it can be replaced for multiple testing with the same plate. This setting is designed to reduce disposable material for a lower cost.

The structural sensor is shown in Fig. 1. It mainly consists of three parts: top load cube plane, middle vertical beam and rigid bottom. Each top cube is independently hold by one vertical supporting beam. We define the combination of one top cube and one supporting beam as a single pressure cell. Depending on the contact surface of the tool which creates the impact force, a number of the pressure cells are affected so that the top cubes will move downwards. Under a specific target pressure, the supporting beam will be destroyed and the top cube will be driven towards the rigid bottom to show an obvious sign of large deformation.

## III. 3D Printing fabrication

In this section, we illustrate the fabrication process according to the design requirements. In order to obtain a disposable structure, we choose 3D printing fabrication process. There are many 3D printers available nowadays. Here, we use a Makerbot Replicator 2X for the fabrication process.

The challenge of the fabrication process is to build a small size feature with a clear outline. As shown in Fig. 3, the structure is well printed. The outline is a acceptable clear square. As described in Section II, the size of the top cube and the gap between the two cubes determine the area of the pressure cell. Furthermore, the area of the pressure cell determines the precision of the measurement. Thus, we need to print as smaller pressure cell as possible. The diameter and length of the supporting beam determine the maximum allowed loading. Well printed supporting beam is needed for the precise measurement. However, the quality of the printed structure is constrained by FDM. If the size of the top cube is too small, the top could not maintain the square shape. The ideal design is shown in Fig. 1(b). However, due to the limitation of FDM 3D printing, the actual shape of the printed sensor is shown in Fig. 3. Careful examination of printed artifact shows the outline of some square reduce to a small polygon. Another feature of FDM is that it prints some special patterns when the feature to be printed reaches the minimum allowed printing size of the 3D printer. For example, this Makerbot printer has a nozzle of 4 $mm$. When the drawing shows a feature of 10 $mm$, the printer has the limitation to print this feature because the dimension 10 is not an multiple of the nozzle diameter 4. Thus, the printer

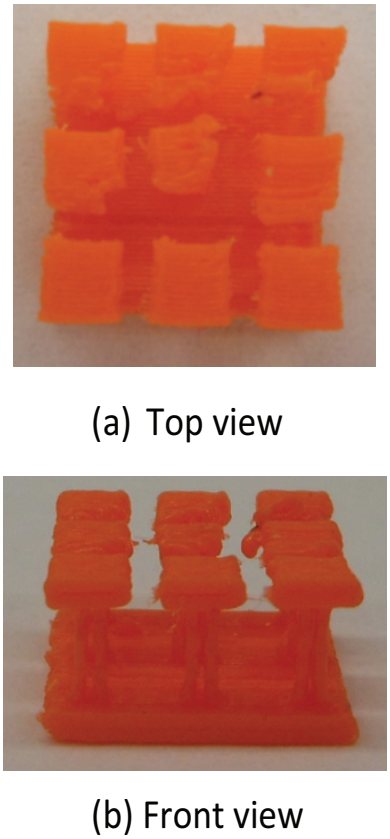


Fig. 3. Structure Fabricated by FDM.

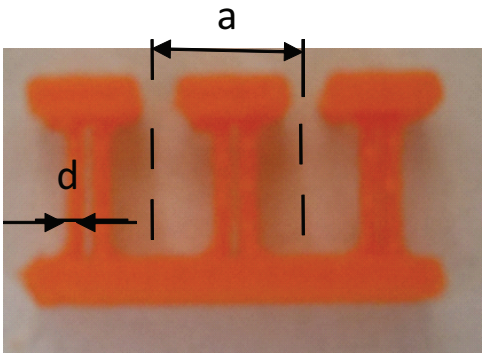


Fig. 4. Two Beam Design through FDM.

will print two separated beams of 4 $mm$ with a gap of 2 $mm$ instead of a monolithic part of 10 $mm$. The two-beam structure is shown in Fig. 4.

With regard to the printing material, we choose the Makerbot Acrylonitrile butadiene styrene (ABS) as the main printing filament. Besides, we also use a supporting material during the printing as show in Fig. 5. The white supporting material is high impact polystyrene (HIPS). The printing extrusion and travel speeds are 100 $m/s$ and 45 $m/s$, respectively. The nozzle size is 0.4 $mm$ in diameter. A well calibrated printer is required to reach the high precision of the printing. Nozzle temperature is set at 230 $^{\circ}C$ for ABS and 250 $^{\circ}C$ for HIPS. Young's modulus of ABS is 2200 $N/mm^2$ and the flexural strength is $37N/mm^2$. An alternative material of ABS is Polylactic acid (PLA), of which Young's modulus is 3500 $N/mm^2$ and the flexural strength is 62 $N/mm^2$. Nozzle temperature is 210 $^{\circ}C$ for

ISBN: 978-988-19253-6-7
ISSN: 2078-0958 (Print); ISSN: 2078-0966 (Online)

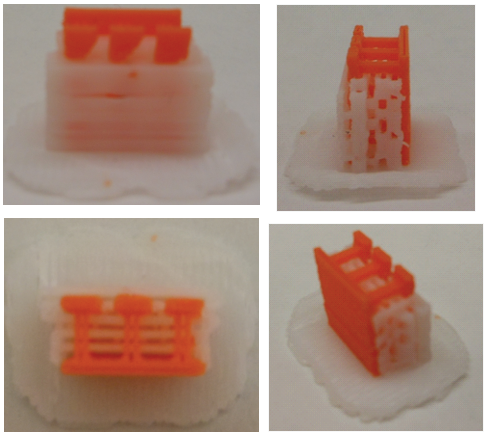

Fig. 5. Supporting Material for FDM.

PLA.

The nozzle of the 3D printer moves continuously in plane while discontinuously in the vertical direction, and this will cause the discontinuity of the printed string in the vertical direction. Because of this phenomena, the model is vertically positioned in Fig. 5 to ensure the supporting beam is well printed with planar motion of the nozzle. In order to print the matrix of the pressure cell, supporting material is used in the printing process. Here, we use HIPS as the supporting material which is dissolved in d-limonene (orange oil) while ABS and PLA is not dissolved in d-limonene. However, ABS is not totally sticky to HIPS when the feature is in a small size. As shown in Fig.5, some cubes are not fully printed because the first layer on HIPS is not well printed. Again, the structural parameters of the design are constrained by the capabilities of the 3D printing method. With a different type of 3D printing technology, the sensor could be built smaller, fine feature, or from different materials. By means of 3D printing with higher resolution, we could reduce the size of top cubes to increase the sensitivity regarding to the size of the object to be measured. For example, SLA commonly has a higher resolution and uses cured material like resin.

## IV. ANALYTICAL MODEL AND STRUCTURAL ANALYSIS

In this section, the design parameters of the structure are illustrated. The maximum allowed force is calculated from the limitation of buckling and flexural strength. The screw theory based stiffness matrix is derived for this sensor structure.

### A. Design parameters

The schematic drawing of the sensor is shown in Fig. 6. Although one supporting beam is shown in the drawing, two beams with diameter of $d$ will be printed if the size is set as 1 $mm$ as we discussed before. Because of this printing feature, we draw a beam with the cross section of $10mm \times 4mm$ to get two identical beams. Because of the printing accuracy, the edge and especially the corner of the rectangular cross section turn to be round. Here, we model the supporting beam with a circular cross section with a diameter $d$. The design parameters include that the gap between the two beams is 0.2 $mm$ and the length $l$ is 4 $mm$. The top cube has a thickness

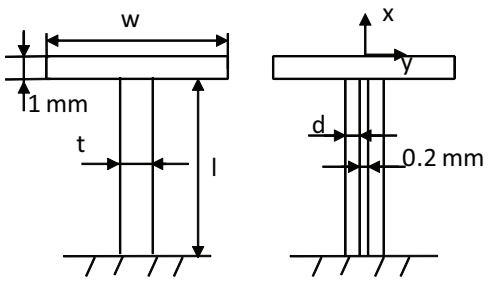


Fig. 6. Schematic Drawing of Single Pressure Cell.

of 1 $mm$ and the length of the edges of the top surface equals to 3 $mm$.

### B. Analytical model derivation

As shown in Fig. 7, we firstly build the coordinate system at the center of the top cube. The pressure to be measured is applied on the top cube so that it creates a vertical force on the vertical supporting beam. According to the Euler' buckling formula, the beam will buckle under a specific force. The force of the buckling noted as the critical load can be derived as

$$F_{cr} = \frac{n\pi^2 EI}{l^2}, \tag{1}$$

where the unit of $F_{cr}$ is $N$. $n$ is the factor accounting for the end conditions, and here $n$ equals to 4 for both ends fixed condition. We assume the pressure here is directly and vertically applied on the top surface. There are not other moments and forces applied ideally. Thus, the received force and moments are considered as the causes of the parasitic errors of the measurement regarding to the main vertical direction. $E$ is the Young's modulus with the unit $N/mm^2$. $l$ is the length of supporting beam and $I$ is the moment of inertia, of which the unit is $mm^4$. Except the buckling status, the beams are also affected by the compression on the cross section. This results in the deformation of the beam along the axial direction. With the accumulated deformation, the beam will fail when the stresses reach the maximum strength. Thus, we also need to examine wether the stress in the cross section of the beam reaches the allowed stress. The maximum allowed force can be derived as

$$F_s = \frac{\sigma_s \pi d^4}{4}, \tag{2}$$

where $F_s$ is the maximum allowed load with regarding to the flexural stress. Here we choose flexural stress, since we consider the 3D printing beam more as a flexural structure. The yield stress is also commonly chose as the standard maximum allowed stress. Another reason is that the material properties of the polymers are much different due to the different fabrication processes, added plasticizers, etc. Here, we use flexural strength also because of the limited information of the material properties from Makerbot. From Eq.(1) and Eq. (2), we can derive the maximum allowed force for a single pressure cell as

$$F_m = min\left(F_{cr}, F_s\right). \tag{3}$$

ISBN: 978-988-19253-6-7
ISSN: 2078-0958 (Print); ISSN: 2078-0966 (Online)

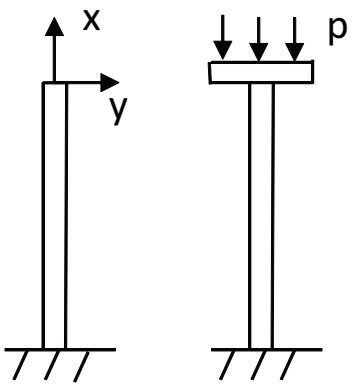


Fig. 7. Analytical Model for the Supporting Beam.

With the material properties, we can know that $F_m$ is 4.65 $N$. With the combination of the two derived force, we calculate the allowed pressure for a single pressure cell as

$$P = \frac{F_m}{a^2}, \tag{4}$$

where $a$ is shown in Fig. 4, which denotes the dimension of a single pressure cell. Thus, we can derive the maximum allowed pressure as 0.52 $N/mm^2$ with the given dimensions. The pressure for this two-beam setting is 1.04 $N/mm^2$. Furthermore, the sensor stiffness in six degrees of freedom (DOF) is also important. For example, the force in the y direction can be considered as a noise. However, this force will also cause the structure to deform. Thus, it is necessary to analyze the stiffness of the structure in 6DOF. Here, we adopt the Screw Theory [9], [10] for the derivation of the stiffness. In the Screw Theory, the deformation is denoted by a general twist vector $\hat{T} = (\theta_x, \theta_y, \theta_z; \delta_x, \delta_y, \delta_z)$ and the loading is denoted by a wrench vector $\hat{W} = (F_x, F_y, F_z; M_x, M_y, M_z)$. The stiffness matrix is defined as $\hat{W} = [\hat{K}]T$. Here, the units of the rotational and translational displacement are $radian$ and $mm$, respectively. The units of force and moment are $N$ and $Nmm$, respectively.

In the stiffness modeling of the sensor structure, the stiffness of a single beam with circular cross section [11] is defined as

$$[C^w] = \frac{l}{EI_z}\begin{bmatrix} 0 & 0 & 0 & \frac{1}{2\chi} & 0 & 0 \\ 0 & 0 & -\frac{l}{2} & 0 & 1 & 0 \\ 0 & \frac{l}{2} & 0 & 0 & 0 & 1 \\ \frac{l^2\eta}{16} & 0 & 0 & 0 & 0 & 0 \\ 0 & \frac{l^2}{3} & 0 & 0 & 0 & \frac{l}{2} \\ 0 & 0 & \frac{l^2}{3} & 0 & -\frac{l}{2} & 0 \end{bmatrix}, \tag{5}$$

where $\eta = d^2/l^2$, $\chi = 1/2(1+\nu)$, $\nu$ is the Poisson's ratio 0.3. By substituting the material properties, the matrix of one single beam can be written as

$$[C^w] = \begin{bmatrix} 0 & 0 & 0 & 1.88 & 0 & 0 \\ 0 & 0 & -2.89 & 0 & 1.45 & 0 \\ 0 & 2.89 & 0 & 0 & 0 & 1.45 \\ 0.14 & 0 & 0 & 0 & 0 & 0 \\ 0 & 7.80 & 0 & 0 & 0 & 2.89 \\ 0 & 0 & 7.80 & 0 & -2.89 & 0 \end{bmatrix}, \tag{6}$$

Here, the value -2.89 means the rotation angle in the y direction with the applied force of 1 $Nmm$ in the z direction and its unit is $radian$. After obtaining the matrix of one beam, we can derive the stiffness matrix of the whole structure. Here, we consider the top platform as a rigid body and there is no deformation in this rigid part. The two beams are determined to be the deformable cube. Because the coordinate system is placed on the center of the top cube, the two beams are considered to be connected in parallel to the top rigid parts. [12]. By means of the adjoint transformation matrix $[Ad]$, we can derive the stiffness of the two beams with the equation of parallel mechanism as

$$[K] = \sum_{i=1}^{2} [Ad_i][K_w][Ad_i]^{-1}, \tag{7}$$

where $[Ad]$ is further defined as

$$[Ad_i] = \begin{bmatrix} R & 0 \\ DR & R \end{bmatrix}. \tag{8}$$

Here, $[D]$ is the skew-symmetric matrix defined by the translational vector $d$ [13], [14]. Because the two beams are placed in the same direction in the coordinate system, there is no rotational matrix for the coordinate transformation. There are only translational coordinate transformations of the two local coordinates to the global origin at the top center. The transformation can be described as

$$[R_1] = [I] \;\; \mathbf{d}_1 = (1, -(d+0.2)/2, 0) \tag{9}$$

$$[R_2] = [I] \;\; \mathbf{d}_2 = (1, (d+0.2)/2, 0) \tag{10}$$

Here, the subscript 1 means the left vertical beam and 2 means the right vertical beam. The final compliance matrix of the a two-beam structure at the origin of the coordinate system can be derived as

$$[C] = \frac{l}{EI_z}\begin{bmatrix} 0 & 0 & 0 & 0.87 & 0 & 0 \\ 0 & 0 & -2.17 & 0 & 0.72 & 0 \\ 0 & 0.22 & 0 & 0 & 0 & 0.72 \\ 0.007 & 0 & 0 & 0 & 0 & 0 \\ 0 & 1.66 & 0 & 0 & 0 & 0.22 \\ 0 & 0 & 7.52 & 0 & -2.17 & 0 \end{bmatrix}, \tag{11}$$

By means of the matrix, we can analyze the stiffness of the parasitic errors of the forces and moments in the three directions. The element of the first row and forth column, 0.87 means the rotational displacement in $radian$ caused by the applied moment in the x direction. Physically, this means the rotational angle of this sensor when a moment applied at the center of the top surface. Because this sensor is designed to only measure the vertical pressure, the compliance matrix is useful to analyze the potential deformation in the real testing.

## V. One Application of the Sensor

This structural pressure sensor is designed to measure a target pressure. In this section, we illustrate one application of the sensor. After being mounted underneath the biosimulant artifact fabricated by the National Institute of Standards and Technology (NIST), the structure can be used to measure the severity of injuries caused in the case of a robot impact with a human.

ISBN: 978-988-19253-6-7
ISSN: 2078-0958 (Print); ISSN: 2078-0966 (Online)

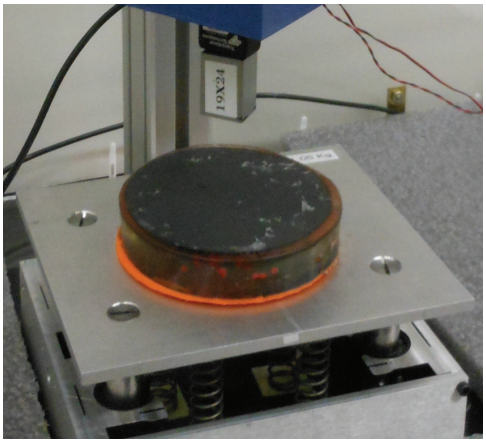

Fig. 8. The Robot Impact Testing.

The movement of manufacturing to countries featuring labor with low hourly wages over the last fifteen years has motivated the development of a new generation of industrial robots that can work side-by-side with human workers [15]. Since most robots are powerful moving machines, the safety of workers working around these robots has become a top priority for safety standards development. Thus, a pressure sensor system is needed for the impact safety testing. The Dynamic Impact Testing and Calibration Instrument (DITCI) [16] is a simple instrument, with a significant data collection and analysis capability that is used for the testing and calibration of the pressure sensor system.

Here, we apply the pressure structural sensors in the whole sensor system designed for the human robot safety impact testing. The sensor system is set on the DITCI instrument stage, as shown in Fig. 8. The whole sensor system includes a top biosimulant artifact [16] and a bottom sensor. As shown in Fig. 9, the sensor system consists of three layers: top leather skin, middle ballistic gelatin and bottom sensor. The bottom layer is the structural sensor, which is mounted underneath the artifact. Then structural sensor is used to measure the pressure of the bottom surface of the ballistic gelatin. Through the measurements of the calibrated bottom structural pressure sensor, we could reconstruct the top impact pressure. The top two layers are called the biosimulant artifact. The biosimulant artifact simulates human skin and muscle and simulates the stress distribution when the impact force is applied on the top of the skin. By studying the distribution of the stress in the ballistic gelatin caused by the dynamic impact force, we can build the relationship of the top impact pressure and the pressure distribution on the bottom surface of the ballistic gelatin.

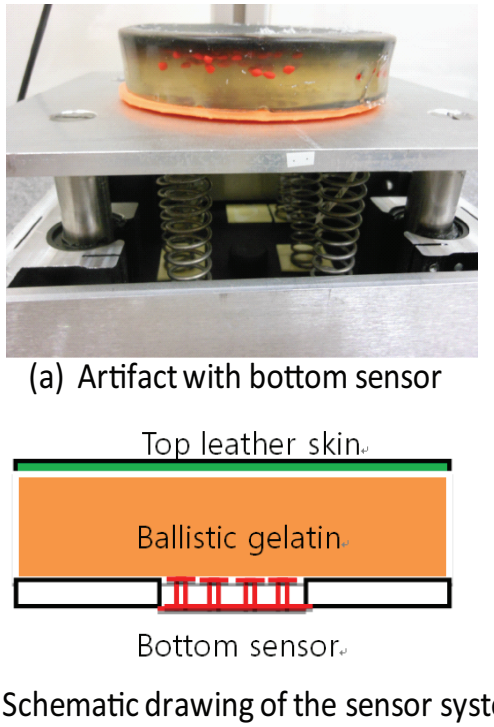


Fig. 9. Sensor System.

## VI. CONCLUSIONS

In this paper, we present a new design of a structural pressure sensor. This sensor adopts 3D printing fabrication to build a small size structure. The vertical beam is used as the measurement part. Some meaningful conclusions can be drawn as following. (1) The design and fabrication process are proposed in the paper. (2) An analytical model is derived to calculate the allowed loading. It is based on the critical force of buckling and the maximum allowed force of the flexural strength. (3) The measurement of the pressure is also decided by the size of the top cube. However, a larger dimension of the top surface will also result in a lower sensitivity of the measurement. (4) The stiffness matrix is derived for the analysis of the structure by means of the Screw Theory. (5) The structural pressure sensor is disposable, low cost, and easy to fabricate. (6) An application example of the sensor is proposed with the combination of the bioartifact fabricated by NIST to measure the impact pressure for robot safety testing.

## REFERENCES

[1] C. Sander, J. W. Knutti, and J. Meindl, "A monolithic capacitive pressure sensor with pulse-period output," *Electron Devices, IEEE Transactions on*, vol. 27, no. 5, pp. 927–930, May 1980.
[2] S. T. I. S. K. Y. K. H. Someya, T. and T. Sakurai, "A large-area, flexible pressure sensor matrix with organic field-effect transistors for artificial skin applications," *PNAS*, vol. 101, no. 27, pp. 9966–9970, 2004.
[3] D. Abeysinghe, S. DasGupta, J. Boyd, and H. Jackson, "A novel mems pressure sensor fabricated on an optical fiber," *Photonics Technology Letters, IEEE*, vol. 13, no. 9, pp. 993–995, Sept 2001.
[4] H. Shi, H.-J. Su, N. Dagalakis, and J. A. Kramar, "Kinematic modeling and calibration of a flexure based hexapod nanopositioner," *Precision Engineering*, vol. 37, no. 1, pp. 117 – 128, 2013.
[5] H. Shi and H.-J. Su, "Workspace of a flexure hexapod nanopositioner," in *Proceedings of ASME IDETC/CIE*, 2012, chicago, Illinois, August 12-15.
[6] J. Palasagaram and R. Ramadoss, "Mems-capacitive pressure sensor fabricated using printed-circuit-processing techniques," *Sensors Journal, IEEE*, vol. 6, no. 6, pp. 1374–1375, Dec 2006.
[7] R. Krondorfer and Y. Kim, "Packaging effect on mems pressure sensor performance," *Components and Packaging Technologies, IEEE Transactions on*, vol. 30, no. 2, pp. 285–293, June 2007.
[8] I. T. Y. T. O. K. Nakamura K., Tomohiro, "Mems pressure sensor," *US Patent*, vol. 8516905 B2, June.
[9] H.-J. Su, H. Shi, and J. Yu, "Analytical compliance analysis and synthesis of flexure mechanisms," in *Proceedings of ASME IDETC/CIE*, 2011, washington, DC, August 28-31.
[10] H. Shi, "Modeling and analysis of compliant mechanisms for designing nanopositioners," Ph.D. dissertation, The Ohio State University, Columbus, OH,USA, 2013.

ISBN: 978-988-19253-6-7
ISSN: 2078-0958 (Print); ISSN: 2078-0966 (Online)

[11] H. Shi and H.-J. Su, "An analytical model for calculating the workspace of a flexure hexapod nanopositioner," *ASME Journal of Mechanisms and Robotics*, vol. 5, no. 4, p. 041009, 2013.
[12] H.-J. Su, H. Shi, and J. Yu, "A symbolic formulation for analytical compliance analysis and synthesis of flexure mechanisms," *ASME Journal of Mechanical Design*, vol. 134, no. 5, p. 051009, 2012.
[13] H. Shi, H.-J. Su, and N. Dagalakis, "A stiffness model for control and analysis of a MEMS hexapod nanopositioner," *Mechanism and Machine Theory*, vol. 80, pp. 246 – 264, 2014.
[14] H. Shi, X. Duan, and H.-J. Su, "Optimization of the workspace of a MEMS hexapod nanopositioner using an adaptive genetic algorithm," in *Robotics and Automation (ICRA), 2014 IEEE International Conference on*, May 2014, pp. 4043–4048, hong kong, May 31-June 7.
[15] E. Guizzo and E. Ackerman, "How rethink robotics built its new baxter robot worker," in *IEEE Spectrum*, 2012.
[16] N. Dagalakis, J. Yoo, and T. Oeste, "Human-robot collaboration dynamic impact testing and calibration instrument for disposable robot safety artifacts."

ISBN: 978-988-19253-6-7
ISSN: 2078-0958 (Print); ISSN: 2078-0966 (Online)